J. Fluid Mech. (2010), *vol.* 644, *pp.* 107–122. © Cambridge University Press 2010
doi:10.1017/S0022112009992242

Reynolds number dependence of mean flow structure in square duct turbulence

ALFREDO PINELLI[1]†, MARKUS UHLMANN[2],
ATSUSHI SEKIMOTO[3] AND GENTA KAWAHARA[3]

[1]Modeling and Numerical Simulation Unit, CIEMAT, 28040 Madrid, Spain

[2]Turbulent Flow Group, Institute for Hydromechanics, University of Karlsruhe, 76128 Karlsruhe, Germany

[3]Department of Mechanical Science, Osaka University, 560-8531 Osaka, Japan

(Received 12 February 2009; revised 14 September 2009; accepted 14 September 2009)

We have performed direct numerical simulations of turbulent flows in a square duct considering a range of Reynolds numbers spanning from a marginal state up to fully developed turbulent states at low Reynolds numbers. The main motivation stems from the relatively poor knowledge about the basic physical mechanisms that are responsible for one of the most outstanding features of this class of turbulent flows: Prandtl's secondary motion of the second kind. In particular, the focus is upon the role of flow structures in its generation and characterization when increasing the Reynolds number. We present a two-fold scenario. On the one hand, buffer layer structures determine the distribution of mean streamwise vorticity. On the other hand, the shape and the quantitative character of the mean secondary flow, defined through the mean cross-stream function, are influenced by motions taking place at larger scales. It is shown that high velocity streaks are preferentially located in the corner region (e.g. less than 50 wall units apart from a sidewall), flanked by low velocity ones. These locations are determined by the positioning of quasi-streamwise vortices with a preferential sign of rotation in agreement with the above described velocity streaks' positions. This preferential arrangement of the classical buffer layer structures determines the pattern of the mean streamwise vorticity that approaches the corners with increasing Reynolds number. On the other hand, the centre of the mean secondary flow, defined as the position of the extrema of the mean cross-stream function (computed using the mean streamwise vorticity), remains at a constant location departing from the mean streamwise vorticity field for larger Reynolds numbers, i.e. it scales in outer units. This paper also presents a detailed validation of the numerical technique including a comparison of the numerical results with data obtained from a companion experiment.

1. Introduction

The turbulent flow through a square duct represents one of the simplest geometrical configurations that exhibit secondary flow of the second kind, as classified by Prandtl (1926). Secondary motions of the second kind are mean flows induced by turbulence fluctuations themselves. The existence of such secondary mean motion in this

---

† Email address for correspondence: a.pinelli@ciemat.es

geometrical configuration is well known since the experiments by Nikuradse (1926), who was the first to measure it indirectly. The mean motion in the streamwise direction is also characterized by a non-negligible deformation of the primary mean velocity profile that presents a non-uniform distribution of the skin friction coefficient along the edges. Previous experimental measurements of the flow in a square duct (Brundrett & Baines 1964; Gessner 1973; Melling & Whitelaw 1976) as well as direct and large eddy simulations (Madabushi & Vanka 1991; Gavrilakis 1992) have provided useful reference data for the mean velocities and the Reynolds stress tensor. Those studies were mainly focused upon the budget of the averaged flow equations, while not providing much information on the underlying physical mechanisms responsible for the formation of secondary flow. Huser & Biringen (1993) attempted to relate the appearance of secondary flow to an interaction of ejection events between adjacent walls in the corner region. In a recent paper (Uhlmann *et al.* 2007), we have considered in detail the case of the marginal Reynolds number regime in this geometry. By marginal regime we mean the limiting behaviour of the turbulent flow at Reynolds numbers on the verge of relaminarization (i.e. bulk Reynolds number in the order of 1100 corresponding to a friction Reynolds number of about 80). In this regime, strong evidence has been presented that the buffer layer coherent structures play a crucial role in the appearance of secondary flow of Prandtl's second kind and in the deformation of the mean streamwise velocity profile. In particular, it has been shown that the deformation of the mean streamwise velocity profile is due to the presence of a persistent low velocity streak preferentially located over the centre of the edges. Also, there exists a matching between the preferential positions of quasi-streamwise vortices flanking the streak and the pattern of the mean secondary vorticity. Similar mean flow patterns have been observed in a recent study (Biau, Soueid & Bottaro 2008) that analysed the time evolution of initial streamwise sub-optimal disturbances at a value of the Reynolds number close to relaminarization. When considering higher Reynolds numbers, other effects may appear. First of all, motions at different scales would play a role, whereas in the low Reynolds number cases the cross-stream scale of coherent structures is comparable with the duct width. Also, the length of the edge of the square cross-section expressed in wall coordinates increases, therefore allowing for the simultaneous presence of multiple pairs of high and low velocity streaks, meaning that in the flow region close to the centre of each edge the flow would behave more and more like a turbulent plane Poiseuille flow without any preferential positioning of the buffer layer structures.

The main motivation of the present paper is to further pursue the idea that the secondary flow is a footprint of the coherent motions embedded in the turbulent flow. Evidence of this conjecture is given by numerical results obtained by direct numerical simulation performed at higher Reynolds numbers (i.e. higher than the marginal one) where several pairs of streaks and associated streamwise vortices can be accommodated simultaneously near each wall (i.e. at the same streamwise location, but separated in the spanwise coordinate). In particular, we propose a scenario in which the position of the centre of the mean secondary vortices (the location of the extrema of the mean streamwise vorticity) is determined by the preferential positioning of quasi-streamwise vortices associated with a high speed streak located close to each one of the corners. On the other hand, the change in the pattern of the mean secondary velocity streamlines is induced by the presence of motions at larger scales. Before introducing and motivating our main conclusions, the numerical code is briefly illustrated together with comparisons with both previous numerical studies and experimental results.

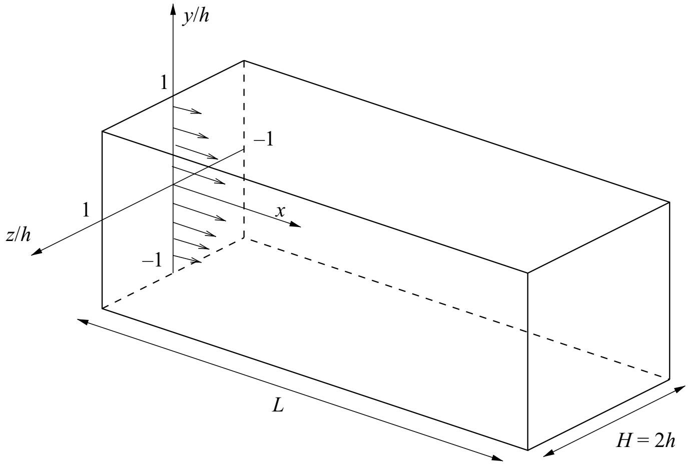

FIGURE 1. Coordinates system and geometry of the duct.

2. Numerical methodology

We are considering an incompressible flow in a duct with a square cross-section and infinite streamwise extension. The Cartesian coordinates are (x, y, z) with x being the streamwise direction and y–z the cross-stream plane $[-h, h] \times [-h, h]$ (see figure 1). The time evolution of the velocity vector $\boldsymbol{u} = (u, v, w)$ (u along x, v along y and w along the z direction) and the pressure p are governed by the incompressible Navier–Stokes equations

$$\partial_t \boldsymbol{u} + \nabla p = -(\boldsymbol{u} \cdot \nabla)\boldsymbol{u} + \frac{1}{Re_b}\nabla^2 \boldsymbol{u}, \tag{2.1a}$$

$$\nabla \cdot \boldsymbol{u} = 0, \tag{2.1b}$$

written in non-dimensional form with density fixed to unity and the Reynolds number, $Re_b = U_b h/\nu$, formed with the bulk velocity U_b, the duct semi-height h and the kinematic viscosity ν. For convenience, we also introduce the definition of the friction Reynolds number as $Re_\tau = u_\tau h/\nu$ with $u_\tau = \sqrt{\tau_w/\rho}$ the friction velocity, where τ_w is the wall shear stress averaged in time and on the four limiting walls and ρ is the constant density. The velocity vector is subject to the no-slip and impermeable conditions at the walls, while periodic conditions are specified at the cross-stream boundary faces.

We employ an incremental-pressure projection method for splitting the system (2.1) into two fractional steps. Using a semi-implicit scheme for the viscous terms and a three-steps low-storage Runge–Kutta method with an explicit treatment for the nonlinear terms, the semi-discrete system can be written as follows:

$$\frac{\boldsymbol{u}^* - \boldsymbol{u}^{k-1}}{\Delta t} = -\gamma_k[(\boldsymbol{u} \cdot \nabla)\boldsymbol{u}]^{k-1} - \zeta_k[(\boldsymbol{u} \cdot \nabla)\boldsymbol{u}]^{k-2} - 2\alpha_k \nabla p^{k-1} + \frac{\alpha_k}{Re_b}\nabla^2\left(\boldsymbol{u}^* + \boldsymbol{u}^{k-1}\right), \tag{2.2a}$$

$$\nabla^2 \phi^k = \frac{\nabla \cdot \boldsymbol{u}^*}{2\alpha_k \Delta t}, \tag{2.2b}$$

$$\boldsymbol{u}^k = \boldsymbol{u}^* - 2\alpha_k \Delta t \nabla \phi^k, \tag{2.2c}$$

$$p^k = p^{k-1} + \phi^k - \frac{\alpha_k \Delta t}{Re_b} \nabla^2 \phi^k, \tag{2.2d}$$

where $k = 1, 2, 3$ is the Runge–Kutta step count (with $k = 0$ equivalent to the previous time step and $k = 3$ being the next time step) and $\boldsymbol{u}^*$ is the predicted intermediate velocity. The auxiliary variable ϕ, sometimes called 'pseudo-pressure', is the projector onto the divergence free space. The boundary condition for ϕ in (2.2*b*) is $\partial \phi^k / \partial n = 0$ for all the Runge–Kutta sub-steps, where n is the normal direction to the wall. The following set of coefficients (Verzicco & Orlandi 1996) leads to overall second-order temporal accuracy for both velocity and pressure in the interior of the computational domain: $\alpha_k = \{4/15, 1/15, 1/6\}$, $\gamma_k = \{8/15, 5/12, 3/4\}$ and $\zeta_k = \{0, -17/60, -5/12\}$. On the walls, due to the use of the fractional step scheme, the no-slip condition is verified up to an error of $O(\Delta t^2 \nu)$. In the worst case (corresponding to the lowest considered Reynolds number), the *slip error* was kept below $10^{-4}\ U_b$ by adjusting the time step Δt accordingly. Flow variables are expanded in space by means of truncated Fourier series in the streamwise direction, while Chebyshev polynomials are used in the two cross-stream directions. The collocation points in the cross-stream directions are the standard Gauss–Chebyshev–Lobatto points, while a grid of equispaced nodes is defined in the streamwise direction. The nonlinear terms in (2.2*a*) are evaluated in physical space, whereas the linear explicit terms are evaluated in spectral space. The fields are transformed back and forth by means of fast Fourier transform (FFT). De-aliasing according to the 2/3-rule is performed in the Fourier direction only. The solution of the Helmholtz equations for the predicted velocity components (2.2*a*) and the Poisson equation for pseudo-pressure (2.2*b*) are carried out in physical space for each streamwise wavenumber by means of a fast diagonalization technique (Haldenwang *et al.* 1984). All the simulated cases have been computed imposing a constant flow rate. To this end, the Fourier zero mode of the streamwise velocity component is adjusted after each Runge–Kutta sub-step in the predictor phase. In particular, an unknown constant pressure gradient A^* is introduced in (2.2*a*) when considering the zero Fourier component of the predicted streamwise velocity $\hat{u}_0^*(y, z)$:

$$\left[\nabla^2 - \frac{Re}{\alpha_k \Delta t}\right] \hat{u}_0^*(y, z) = \hat{F}_0(u^{k-1}, u^{k-2}, p^{k-1}) + A^*, \tag{2.3}$$

where $\hat{F}_0$ contains all the contributions from explicit terms in (2.2*a*) to the zero mode. The solution of problem (2.3) is decomposed as a linear combination of two contributions. The first one $\hat{u}_0^1$ is the solution of (2.3) with $A^* = 0$, while the second $\hat{u}_0^2$ is obtained solving the problem

$$\left[\nabla^2 - \frac{Re}{\alpha_k \Delta t}\right] \hat{u}_0^2(y, z) = 1. \tag{2.4}$$

Both solutions are obtained using Dirichlet homogeneous conditions on the square boundary. The final solution is assembled as

$$\hat{u}_0^*(y, z) = \hat{u}_0^1 + A^* \hat{u}_0^2, \tag{2.5}$$

with A^* obtained from the requirement:

$$Q_f = \int_\Omega \hat{u}_0^1 \, \mathrm{d}y \, \mathrm{d}z + A^* \int_\Omega \hat{u}_0^2 \, \mathrm{d}y \, \mathrm{d}z, \tag{2.6}$$

with $Q_f = 4\ h^2\ U_b$ the desired flow rate through section Ω.

3. Validation

With the aim of validating the numerical method outlined in the previous section, we present a comparison of our results with both reference numerical results and a set of experimental data. In particular, we have considered a fully turbulent case at $Re_b = 2205$, as previously simulated by Gavrilakis (1992), and another case at a slightly higher Reynolds number (i.e. $Re_b = 3535$) for which a set of experimental data (Kawahara *et al.* 2000) is available. Both simulations were performed with a streamwise period of $L_x/h = 4\pi$, which can be considered sufficiently long in order to allow for an adequate decay of the two-point velocity correlations (Gavrilakis 1992, figure 3). For the lower Reynolds number case, we used 128 Fourier modes, corresponding to a streamwise grid spacing of $\Delta x^+ = 14.7$ (here and in the following, the superscript '+' stands for wall units: $l^+ = l/\delta_v$ with $\delta_v = \nu/u_\tau$ the viscous length scale); 97 Chebyshev modes are employed in each cross-stream direction, leading to a spacing of $0.08 \leqslant \Delta y^+, \Delta z^+ \leqslant 4.9$. The time step was fixed at $\Delta t\, U_b/h = 1.93 \times 10^{-2}$, approximately corresponding to a $CFL = 0.22$. Statistics were accumulated over an interval of $t_{stat}\, U_b/h = 8000$. It is worth mentioning that the time accumulated to compute statistical quantities is significantly larger than the one presented in the reference work (Gavrilakis 1992). In order to confirm that the actual streamwise discretization was fine enough to capture the behaviour of typical buffer layer structures, higher resolution computations have been undertaken at $Re_b = 2205$ using 192 Fourier modes in the streamwise direction ($\Delta x^+ < 10$). No substantial difference (less than 4 %) has been found in the second-order statistics of the velocity field. For the higher Reynolds number case, 192 Fourier modes were employed in the streamwise direction leading to the same wall coordinates spacing as in the previous case. In the cross-stream plane, 129 nodes were used in both wall normal directions obtaining a grid spacing of $0.07 \leqslant \Delta y^+, \Delta z^+ \leqslant 5.2$. The temporal resolution was $\Delta t\, U_b/h = 0.5 \times 10^{-3}$. Statistics for the second case were accumulated over a period of $t_{stat}\, U_b/h = 5800$. Details about the reference cases can be found in Gavrilakis (1992) and Kawahara *et al.* (2000). In what follows we give a brief summary of the latter since the original work has never been published in English. The set of data was collected from experiments conducted in a fully developed turbulent flow in a straight water-duct (kinematic viscosity $\nu = 0.94 \times 10^{-2}\,\mathrm{cm^2\,s^{-1}}$). The duct has a square cross-section of an internal width $2h = 100\,\mathrm{mm}$ and length 9 m. The bulk velocity in the duct was set at a value of $U_b = 6.6\,\mathrm{cm\,s^{-1}}$ leading to a Reynolds number of $Re_b = U_b h/\nu = 3535$. A *Dantec* model *60X* two-component LDV system was used to obtain the instantaneous axial and wall-normal velocity components at 37×40 positions in one quadrant of the full cross-section 136 h downstream of the duct inlet. The spanwise component was also obtained from the wall-normal one under the assumption of symmetry with respect to the corner bisector of the duct. The laser light source of the LDV system is 6 W Argon-ion laser *Spectra-Physics 2017*, and Doppler signals were processed by *Dantec* burst spectral analyzer *57X20, 57X35*. The dimension of the measuring volume was $48\,\mu\mathrm{m} \times 48\,\mu\mathrm{m} \times 399\,\mu\mathrm{m}$ in the axial, wall-normal and spanwise directions, respectively. At each measuring position, the data rate of Doppler signals ranged from 100 Hz to 200 Hz, and the total number of the signals was 10^5–1.2×10^5.

Next, we present a comparison of the aforementioned reference data (numerical and experimental) with results obtained with our DNS. All the comparisons will be provided in external units because of the experimental uncertainties in determining the skin friction velocity in the experiments. First, we compare and characterize the mean flow. Figure 2(a) shows a nearly perfect collapse of our mean streamwise

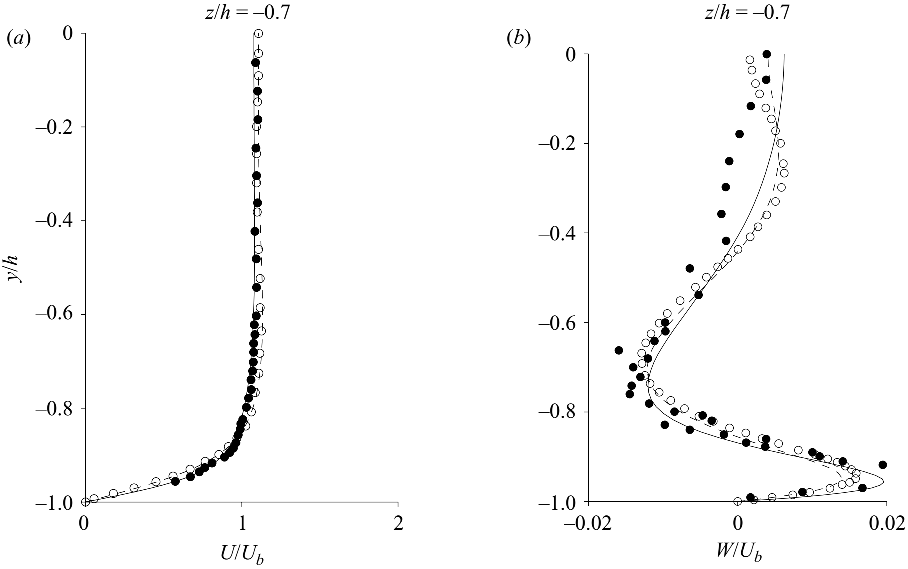

FIGURE 2. Mean velocity components at $z/h=-0.7$: streamwise component (*a*) and cross-stream component (*b*). Present DNS results (—— $Re_b=3500$ ---- $Re_b=2205$) compared with reference DNS data (○) and experimental data (●).

velocity profile (here and throughout the rest of the paper, the operator $\langle\ \rangle$ stands for time and streamwise average) as compared with reference data at section $z/h=-0.7$. At the same section, the profiles of the mean cross-stream velocity component are provided in figure 2(*b*). A certain level of disagreement with the experimental data is clearly visible far from the wall. Nonetheless, in the core region $\langle w \rangle$ is orders of magnitude smaller than U_b. Therefore, even small deformation of the turbulence field by an uncertainty problem in the experimental apparatus could significantly affect the results.

Next, we compare the profile of the normal Reynolds stresses. In figures 3(*a*) and 3(*b*), profiles of the root mean square (rms) of streamwise velocity fluctuations (i.e. $u'=u-\langle u \rangle$) from our DNS are compared with the reference data at two different positions along the edge. A similar set of profiles, at the same locations, for the *rms* of the transversal velocity component ($w'=w-\langle w \rangle$) is given in figures 3(*c*) and 3(*d*). Our DNS results for the normal Reynolds stresses are in excellent agreement with the experimental data. The comparison with the data of Gavrilakis (1992) again yields a very close match. Small discrepancies are probably due to the fact that the time interval during which the statistics were accumulated was substantially shorter in the study of Gavrilakis.

4. Reynolds number dependence

Despite extensive study of the turbulent flow in a square duct using a variety of numerical techniques, there remain significant questions about the scaling properties of the mean secondary flow and the associated distortion of the mean streamwise velocity profile. In what follows we will address the scaling of characteristic positions related to cross-stream and streamwise mean motion within a range of marginal to low Reynolds numbers ($Re_b \leqslant 3500$). In this framework we will propose a physical

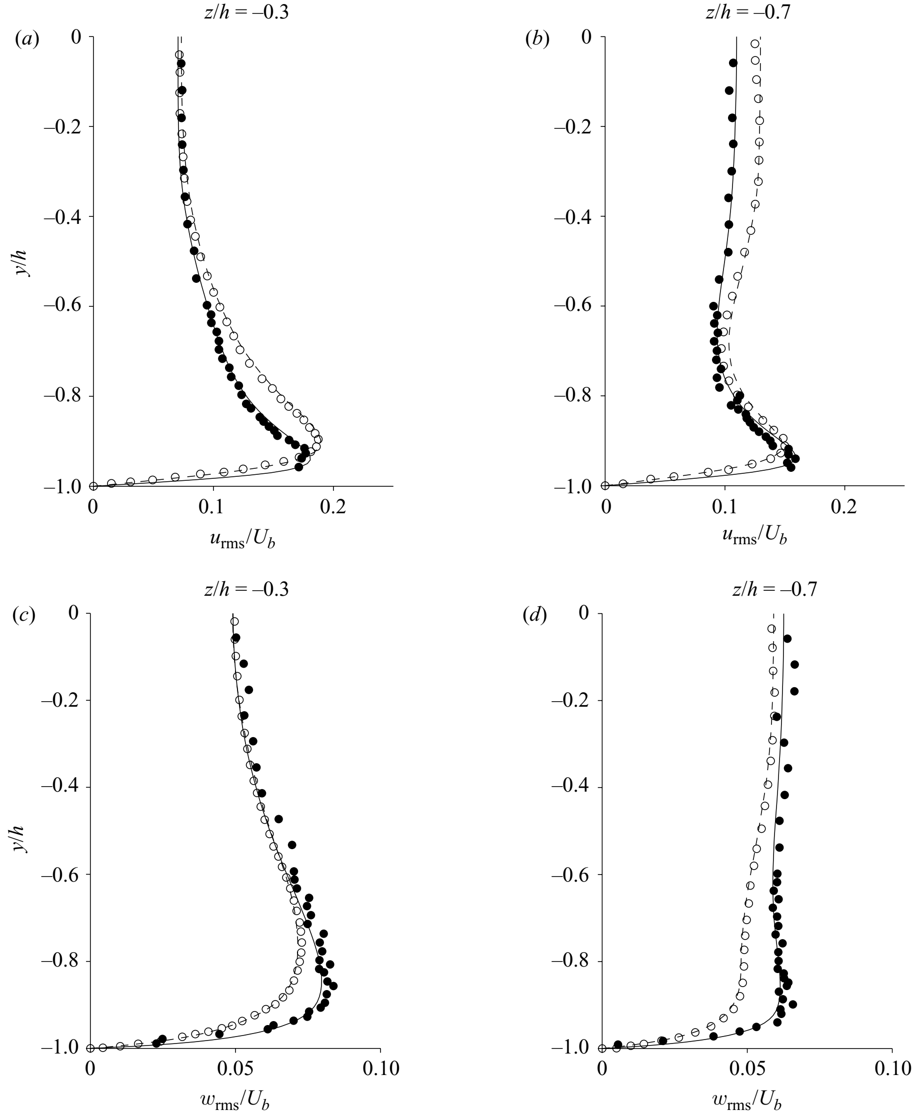

FIGURE 3. Profiles of the rms of the streamwise and cross-stream velocity components at two different positions along one edge. Streamwise component, $\langle u'u' \rangle^{1/2}/U_b$, at $z/h = -0.3$ (*a*) and at $z/h = -0.7$ (*b*). Cross-stream component, $\langle w'w' \rangle^{1/2}/U_b$, at $z/h = -0.3$ (*c*) and at $z/h = -0.7$ (*d*). Lines and symbols are the same as in figure 2.

explanation, in terms of coherent structure dynamics, of the pattern and scaling of the mean secondary motion.

All the simulations have been carried out in a careful manner with a time step such that $CFL \leqslant 0.25$ while keeping the slip error below $0.5 \times 10^{-4}\ U_b$ and by choosing the number of collocation nodes to guarantee a grid spacing verifying $\Delta x^+ \leqslant 15$ and $0.05 \leqslant \Delta y^+ \leqslant 5$ (same spacing criterion for Δz^+). Statistical quantities were accumulated over time intervals $t_{stat}\, U_b/h \geqslant 7000$. Also, all the computations have been carried out using comparable domain sizes: $[-1, 1] \times [-1, 1] \times L_x/h$, with $L_x = 10.97$–$12.57\ h$.

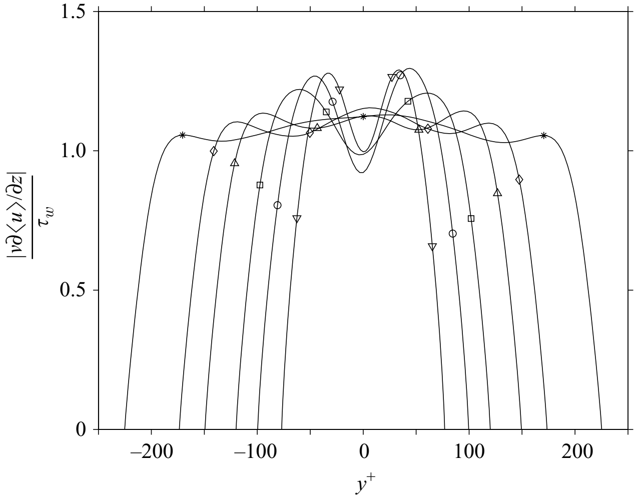

FIGURE 4. Mean local wall stress, normalized by the average over the whole wall, as a function of the distance along the wall in wall units. Symbols indicate the value of the bulk Reynolds numbers: ▽, $Re_b = 1077$; ○, $Re_b = 1400$; □, $Re_b = 1753$; △, $Re_b = 2205$; ◇, $Re_b = 2600$; *, $Re_b = 3500$.

4.1. *Mean streamwise structure*

Firstly, in order to characterize the shape of the mean streamwise profile, we present in figure 4 the mean local wall stress along one edge in wall coordinates. The skin friction coefficients, obtained averaging in time and along the streamwise direction, are in good agreement with the empirical formula: $f^{-1/2} = 2\log_{10}(2.25\, Re_b\, f^{1/2}) - 0.8$, where f is the skin friction factor defined by $f = 8u_\tau^2/U_b^2$ (Jones 1976). At this level, note that the above empirical formula estimates that the length of the edge of the square in wall units spans the range $2h^+ \in [160, 450]$ for the considered interval of Reynolds numbers (i.e. $Re_b \in [1077, 3500]$). From the dimension of the square, expressed in wall units, one may anticipate an upper bound for the number of wall velocity streaks statistically facing each one of the four walls since the average distance between streaks of different velocity sign is of the order of 50^+ (Kim, Moin & Moser 1987). Therefore, for the lowest Reynolds number, one would expect an arrangement of a maximum of three velocity streaks, while for the highest an arrangement of a maximum of nine velocity streaks can be anticipated. Indeed, this argument is confirmed by figure 4. At the lowest values of the Reynolds number the profiles present two maxima and one minimum, indicating that a low velocity streak, flanked by two high velocity ones, is located preferentially at the centre of the edge. At $Re_b = 2205$ and $Re_b = 2600$, the situation changes since now the edge, measured in wall units ($2h^+ \simeq 300$ and $\simeq 350$, respectively), can host up to five streaks of different sign. Figure 4 reveals that the sequence is, from one corner to the mid edge location, high-low-high with a high velocity streak located preferentially close to the centre of the edge. At even higher Re_b more extrema can be detected but their values far from the corners have a clear trend to smooth out approaching the wall-averaged mean value. On the other hand, a persistent fast streak is always detected close to the corner (seen in figure 4 close to the extrema). The reason for the flattening of the local mean skin friction coefficient is strongly related to the relaxation of the aforementioned geometrical constraint: at very low Reynolds number the positioning

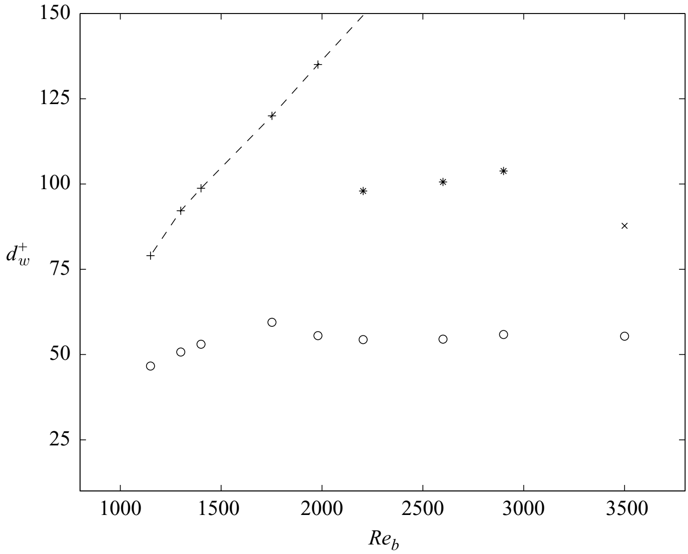

FIGURE 5. Distance to the corner d_w^+, in wall units, of the location along the edge of maximum and minimum of τ_w closest to the corner as a function of Re_b. Here $\circ$ is the position of maximum shear and the crosses represent the position of the location of minimum shear. Different crosses are used to highlight the discrete behaviour of low velocity streak positioning. The dashed line is duct half-width in wall units h^+ as a function of Re_b.

of the streaks is imposed by the geometry; when increasing the Reynolds number, the probability of finding either a high or a low velocity streak at a certain edge position, except in the corner region, becomes more and more uniform like in the case of a turbulent Poiseuille flow. The discrete dependency of the number of allowed streaks as a function of the Reynolds number also reflects upon the distance to the corner of the high and low velocity streaks closest to it. As can be seen in figure 5, at low Reynolds numbers (i.e. $1077 \leqslant Re_b \leqslant 2000$) the low velocity streak is preferentially located at the centre of the edge, since the half-width of the edge, scaled in wall units h^+, increases correspondingly. The location of maximum shear has a clear trend to level off with increasing Re_b at a value of about 50^+ units. On the other hand, at approximately $Re_b = 2000$ (corresponding to $Re_\tau \simeq 120$), the position of the minimum has a sharp change indicating that the wall, above this value, is hosting an average of five streaks. At higher Reynolds numbers, other jumps will probably appear consistently with the appearance of more velocity streaks on average along the edge. As further evidence of preferential streak locations as a function of Reynolds number, in figure 6 the time evolution of the location of low speed streaks along one edge is given in viscous coordinates at different bulk Reynolds numbers. These locations are instantaneously identified as the position of the minimum values of streamwise averaged wall shear stress. It can be seen that at the lowest Reynolds number a single low speed streak smoothly meanders about the centre of the edge. When increasing the Reynolds number more than one simultaneous streak is detected. At the highest Reynolds number the path followed by the low speed streaks becomes less and less predictable without displaying any favourite positioning. This behaviour is consistent with the observed flattening of the local mean skin friction of figure 4. Also, regions close to the corners (i.e. $y^+ \simeq \pm 200$) are seldom visited by low speed streaks. A more quantitative analysis can be obtained by considering the probability density function

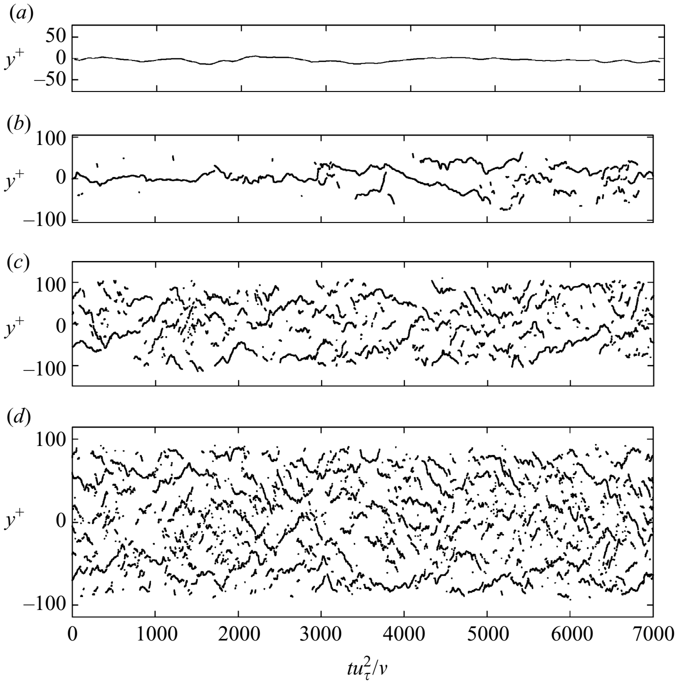

FIGURE 6. Time evolution of position of minimum of the streamwise averaged wall shear stress at $z/h = 1$: (*a*) $Re_b = 1100$, (*b*) $Re_b = 1500$, (*c*) $Re_b = 2205$ and (*d*) $Re_b = 3500$.

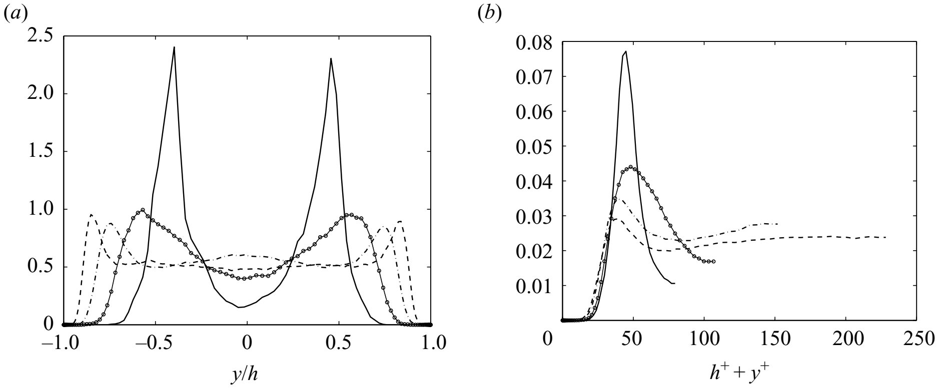

FIGURE 7. Probability density function of low speed streak positions computed considering the instantaneous location of the minimum value of wall skin friction: (*a*) in outer units and (*b*) in inner units (the origin has been translated to the corner). Lines correspond to: ——, $Re_b = 1100$; —●—, $Re_b = 1500$; – · – · – , $Re_b = 2200$; - - - -, $Re_b = 3500$.

(p.d.f.) of the positioning of low and high speed streaks along the edge together with their intensities. In figure 7, the p.d.f. of the locations of low velocity streaks is presented in both outer and inner units. It is observed that an increase of the Reynolds number has the effect of equidistributing the probability of finding a low speed streak along the edge, except close to the corner region where the probability goes to zero, irrespective of the Reynolds number. Also, it can be noticed that the appearance of new local extrema in the p.d.f. is consistent with the jumps in the locations of

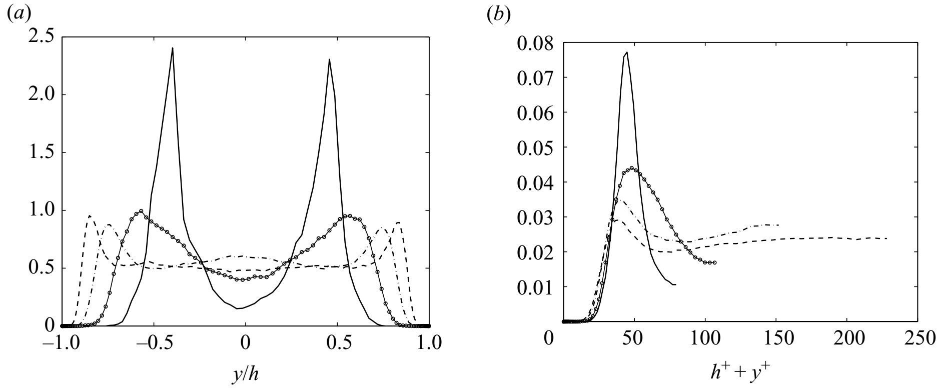

FIGURE 8. Probability density function of high speed streak positions computed considering the instantaneous location of the maximum value of wall skin friction: (*a*) in outer units and (*b*) in inner units (the origin has been translated to the corner). Lines and symbols are as in figure 7.

the distance to the corner of the point of minimal wall shear when increasing the Reynolds number (see figure 5). In figure 8, the same analysis as in figure 7 is given for the high velocity streaks. At the lowest value of Re_b the most probable scenario is two high velocity streaks flanking a low velocity one preferentially located at the edge midpoint. As for the case of low velocity streaks, when increasing Reynolds number the probability of finding a high velocity streak along the edge becomes more and more uniform. The only locations that display a higher probability of hosting high speed streaks are the corner regions as opposed to the preferential absence of low velocity ones.

4.2. *Mean crossflow structure*

When focusing upon the mean value of the cross-stream velocity components, the well known pattern of mean secondary flow in the cross-plane of the square duct consisting of eight vortices, one counter-rotating pair being located above each of the four wall planes is observed. Their sense of rotation is such that the secondary flow on the diagonals is directed towards the corners (Gavrilakis 1992). Figure 9 displays isolines of the mean cross streamfunction $\langle\psi\rangle(y,z)$ computed from $\nabla^2\langle\psi\rangle(y,z)=-\langle\omega_x\rangle$ for three different Reynolds numbers ($Re_b=1077$, $Re_b=2205$ and $Re_b=3500$). Qualitatively, the figure shows that the pattern of the secondary cross mean flow is more and more stretched as Re_b increases. A possible conjecture to explain the distortion of the mean cross motion can be given in terms of superposition of contributions from instantaneous streamwise vorticity at different scales. At the lowest Reynolds number value, the flow is marginally turbulent: production and dissipation scales are not separated and their statistical footprint leads to a smooth secondary flow as shown by Uhlmann *et al.* (2007). At higher Reynolds number values, vortical structures on a wider scale range appear. A lower bound for these structures are the quasi-streamwise vortices associated with near-wall velocity streaks (dissipation scale). An upper bound is determined by the geometrical constraints (largest scales). In figure 10, contours of $\langle\omega_x\rangle(y,z)$ are given at the same three Reynolds numbers considered in figure 9. At $Re_b=1077$, the pattern of mean streamwise vorticity resembles that of the mean streamfunction, except for the layer of mirrored wall vorticity. At higher Re_b values, the shapes of mean streamwise vorticity and

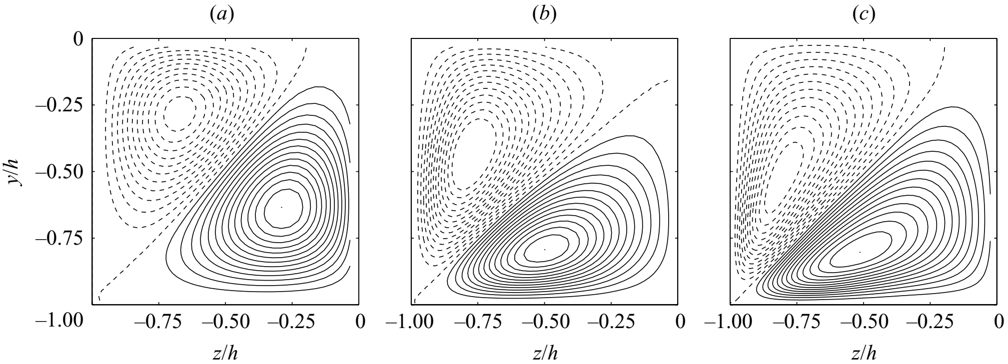

FIGURE 9. Streamlines $\langle\psi\rangle(y,z)$ of secondary mean flow computed using $\langle v\rangle$ and $\langle w\rangle$ averaged over all quadrants (with increment $[\max\langle\psi\rangle - \min\langle\psi\rangle]/30$). Dashed lines correspond to clockwise rotation and continuous lines to counterclockwise motion. (*a*) $Re_b = 1077$; (*b*) $Re_b = 2205$ and (*c*) $Re_b = 3500$. Only $[-1,0]\times[-1,0]$ quadrant is shown.

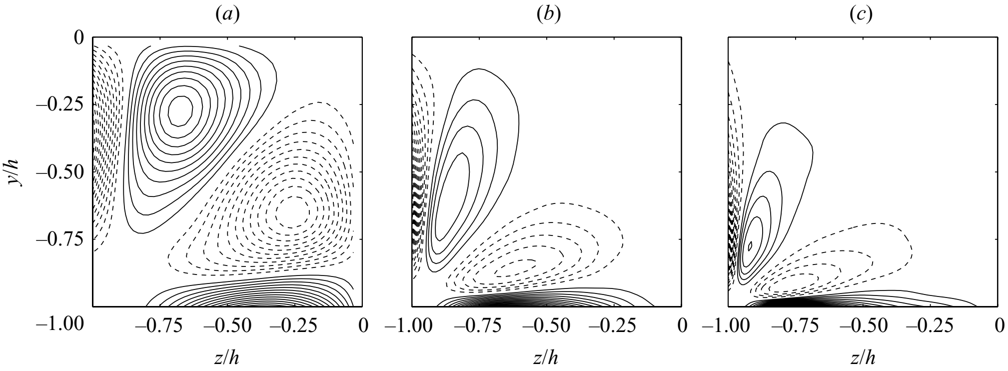

FIGURE 10. Iso-contours of $\langle\omega_x\rangle(y,z)$ of secondary mean flow averaged over all quadrants (with increment $[\max\langle\omega_x\rangle - \min\langle\omega_x\rangle]/30$). Dashed lines correspond to negative values and continuous lines to positive ones. (*a*) $Re_b = 1077$; (*b*) $Re_b = 2205$ and (*c*) $Re_b = 3500$. Only $[-1,0]\times[-1,0]$ quadrant is shown.

streamfunction progressively depart from each other. In particular, the vortex centres and the stagnation points display a completely different behaviour.

A more quantitative analysis of the dependence of the extrema of $\langle\omega_x\rangle(y,z)$ and $\langle\psi\rangle(y,z)$ upon the Reynolds number is shown in figures 11 and 12. Here, the positions of the extrema in terms of distance from the wall at $z/h = -1$ and at $y/h = -1$ of the mean isolines below the bisector in the quadrant $[-1,0]\times[-1,0]$ are given in both external and wall coordinates as a function of Re_b and Re_τ. It is clearly observed that when increasing the Reynolds number the location of the extrema of mean vorticity and streamfunction separates. Also, the discrete change of the number of allowed streaks along the edge, as previously discussed, reflects clearly in the jump of the tangential distance (i.e. the distance to $z/h = -1$) of the minimum of $\langle\omega_x\rangle$ at $Re_b \simeq 2000$ ($Re_\tau \simeq 150$) as reflected in figure 11(*a*, *b*). This observation provides further evidence that the pattern of the mean streamwise vorticity is associated with the near wall coherent structures. Indeed, the position of the minimum of the mean streamwise vorticity has a clear trend to scale with viscous units, indicating a dependence on the wall structures. Moreover, the distance to the wall at $z/h = -1$ expressed in viscous

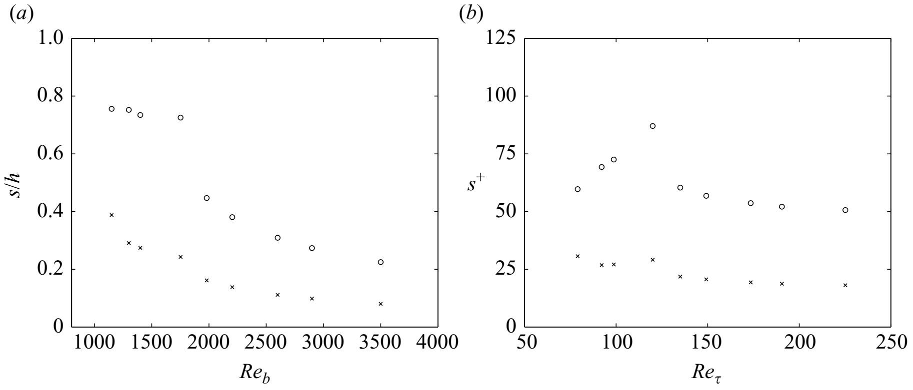

FIGURE 11. Positions of extrema of $\langle \omega_x \rangle$: (a) external coordinates vs. Re_b and (b) wall coordinates vs. Re_τ. Symbols: ○ distance to $z/h = -1$; × distance to $y/h = -1$ (see dashed lines in figure 10).

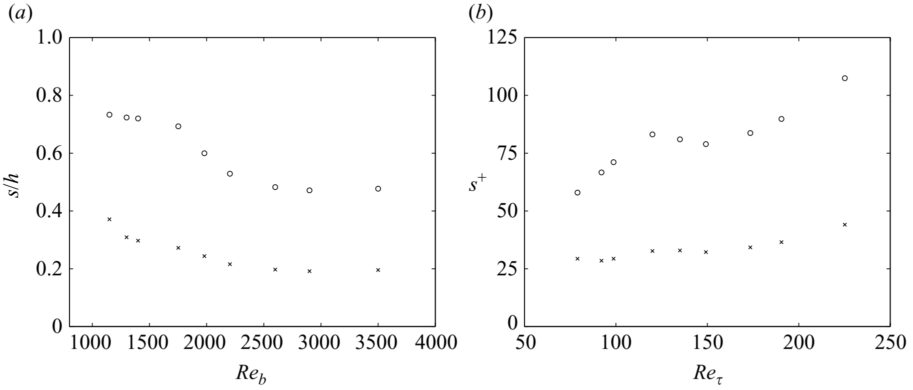

FIGURE 12. Positions of extrema of $\langle \psi \rangle(y, z)$: (a) external coordinates vs. Re_b and (b) wall coordinates vs. Re_τ. Symbols: ○ distance to $z/h = -1$; × distance to $y/h = -1$ (see solid lines in figure 9).

units remains relatively constant and approximately corresponds to the position of the maximum of $\langle \omega_x' \ \omega_x' \rangle$ in a plane channel flow (Jiménez & Moin 1991) that is located between 20^+ and 30^+.

When considering the locations of the extrema of the streamfunction at higher Reynolds numbers, a different behaviour is found. The normal distance of the stagnation point scales in external units (see figure 12). Such a behaviour of the stream function of the mean cross components of velocity when increasing Re_b suggests that organized large-scale velocity structures may participate in determining the shape of the mean secondary crossflow. The large-scale motions are, of course, bounded in size by the geometrical dimension of the duct and, therefore, one may expect the mean cross-stream motion to display patterns that scale with the dimension of the cross-section independent of the value of Re_b.

Further evidence of the direct relation between coherent structures and mean secondary vorticity can be provided by carrying out a vortex eduction study. Here we extend the analysis of Uhlmann *et al.* (2007) to higher Reynolds numbers. In particular, we have detected coherent vortices in each cross-sectional plane of a

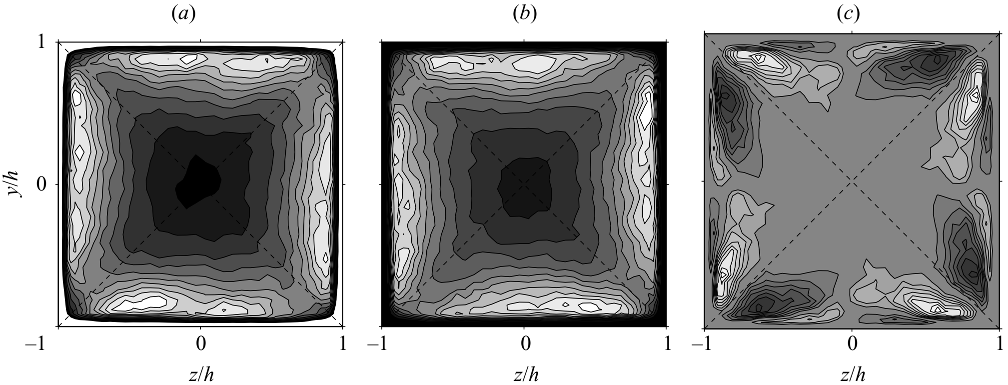

FIGURE 13. Statistical data for the case with $Re_b = 2205$ and $L_x/h = 4\pi$, accumulated from 1000 flow fields over a time interval of $1000h/U_b$. (*a*) Grey levels indicate .1(.1).9 times the maximum probability of occurrence of vortex centres with *negative* streamwise vorticity (white maximum, black minimum); (*b*) the probability for vortices with *positive* streamwise vorticity; (*c*) the difference of the probabilities of the location of positive (*b*) and negative vortex centres (*a*) averaged on the four quadrants (replicated on each quadrant for convenience).

number of instantaneous flow fields by means of the criterion proposed by Kida & Miura (1998): vortex cores are detected by identifying low pressure regions with an additional condition for swirling motion. The educed positions of coherent vortex centres have been stored together with the corresponding local value of the streamwise vorticity for a Reynolds number of $Re_b = 2200$. The resulting probability of occurrence of negative vortex centres is shown in figure 13(*a*). In figure 13(*b*) the occurrence of positive vortex centres is displayed. Finally, in figure 13(*c*) the algebraic difference, averaged over the four quadrants, of the p.d.f. given in figures 13(*a*) and 13(*b*) is shown. The original difference (not shown) is relatively noisy, which stems from the fact that we are computing a field quantity from a discrete set of vortex centres. For this reason, we have computed the mean between the quadrants. We observe that the local maxima of the p.d.f. of the vortex positions, when taking into account the sign of rotation, indicate a strong probability of having two counter-rotating vortices in the corner region, bearing a clear resemblance to the mean secondary flow vorticity pattern accumulated over the same interval (see figure 10*b*). This observation confirms that the mean streamwise vorticity pattern is a statistical portrait of the most probable locations of the quasi-streamwise vortices that are preferentially located in the corner regions. Furthermore, figure 13(*c*) presents a distribution of the p.d.f. in the close-to-the-wall regions, consistent with the fact that, at this Reynolds number (i.e. $Re_b = 2200$), the most probable configuration on each edge is of two stronger high velocity streaks close to the corners and a milder one at the edge centre (see figure 8 and the p.d.f. values at the wall bisector in figure 13*c*). Indeed, the preferential location of the quasi-streamwise vortices (two counter-rotating cores for each octant) induces a preferential positioning of fast velocity streaks in the same regions.

5. Conclusions

We have presented a numerical technique to simulate turbulent flows in infinitely long square ducts at constant flow rate. The numerical method has been validated against data from reference DNS and laboratory experiments.

Our analysis of the DNS results has focused upon the dynamical mechanisms that lead to the behaviour of mean velocity values when increasing the Reynolds number: the deformation of the mean streamwise velocity and the shape of mean secondary flow. It has been found that the mean streamwise velocity component depends upon the number of statistically allowed velocity streaks in the square. When increasing the Reynolds number the variation of wall shear along the spanwise coordinate smoothes out gradually except in the corner region where low velocity streaks are inhibited. In order to understand the scaling of the mean cross-stream velocity components, we have considered the behaviour of both the mean streamwise vorticity and the mean cross-stream function. The two quantities are shown to collapse at the lowest Reynolds number while progressively departing from each other when increasing the Reynolds number value. Evidence has been given that mean streamwise vorticity strongly depends upon statistically preferred location of the quasi-streamwise vortices associated with the pair of fast/slow streaks closest to the corner. Therefore a viscous scaling can be stated for such a mean quantity. On the other hand it has been found that the positions of the stagnation points of the mean crossflow streamfunction do not scale in viscous units but rather in external ones.

The difference between the behaviour of mean streamwise vorticity and mean streamfunction in the crossflow plane stems from the fact that the latter is obtained as the solution of a Poisson equation ($\nabla^2\langle\psi\rangle = -\langle\omega_x\rangle$) with the former as right-hand side. Therefore, the streamfunction exhibits non-local behaviour (i.e. vorticity at any location influences the streamfunction everywhere), much alike the dependence between the pressure field and the divergence of the convective terms. As a consequence, there is no obvious reason why both quantities should scale equally. The precise implications of the relation between mean vorticity and streamfunction in duct flow, however, are beyond the scope of this paper.

Within the considered range of Reynolds numbers, evidence has been given that the mean properties of the flow field depend upon the preferred positioning of buffer layer coherent structures. In particular, below $Re_b \simeq 2000$ all the flow scales collapse, thus making all the mean quantities a direct footprint of the actual most probable location of those structures: mean streamwise vorticity, mean cross-stream function and the loci of the extrema of wall shear stress. At bulk Reynolds numbers higher than 2200, the influence of the coherent structures just reflects in the shape of the mean streamwise vorticity field and in the location of the local maximum of wall stress closest to the corner. The range of Re_b around 2100 is a *transitional* regime in which the region facing the edge bisector starts behaving like a plane channel flow.

In this range of Reynolds numbers, the shape of the mean streamwise vorticity field, the local maximum of the wall shear near the corner, the local maximum of the wall shear on the wall bisector and the local minimum of the wall shear near the corner can be related to the distribution of the coherent structures.

To further investigate the eventual role of other, larger scales upon the mean flow structure higher Reynolds number, simulations will be undertaken in the future.

The collaboration between the groups was supported by the centre of Excellence for Research and Education on Complex Functional Mechanical Systems (COE program of the Ministry of Education, Culture, Sport, Science, and Technology of Japan). M.U. was supported by the Spanish Ministry of Education and Science under contract DPI-2002-040550-C07-04. G.K. was partially supported by a Grant-in-Aid for Scientific Research (B) from the Japanese Society for the Promotion of Science.

REFERENCES

Biau, D., Soueid, H. & Bottaro, A. 2008 Transition to turbulence in duct flow. *J. Fluid Mech.* **596**, 133–142.

Brundrett, E. & Baines, W. 1964 The production and diffusion of vorticity in duct flow. *J. Fluid Mech.* **19**, 375–394.

Gavrilakis, S. 1992 Numerical simulation of low-Reynolds-number turbulent flow through a straight square duct. *J. Fluid Mech.* **244**, 101–129.

Gessner, F. 1973 The origin of secondary flow in turbulent flow along a corner. *J. Fluid Mech.* **58**, 1–25.

Haldenwang, P., Labrosse, G., Abboudi, S. & Deville, M. 1984 Chebyshev 3-d spectral and 2-d pseudo-spectral solvers for the Helmholtz equation. *J. Comput. Phys.* **55**, 115–128.

Huser, A. & Biringen, S. 1993 Direct numerical simulation of turbulent flow in a square duct. *J. Fluid Mech.* **257**, 65–95.

Jiménez, J. & Moin, P. 1991 The minimal flow unit in near-wall turbulence. *J. Fluid Mech.* **225**, 213–240.

Jones, O. 1976 An improvement in the calculation of turbulent friction in rectangular ducts. *ASME J. Fluids Engng* **98**, 173–181.

Kawahara, G., Ayukawa, K., Ochi, J., Ono, F. & Kamada, E. 2000 Wall shear stress and Reynolds stresses in a low Reynolds number turbulent square duct flow. *Trans. JSME B* **66** (641), 95–102.

Kida, S. & Miura, H. 1998 Swirl condition in low-pressure vortices. *J. Phys. Soc. Japan* **67** (7), 2166–2169.

Kim, J., Moin, P. & Moser, R. D. 1987 Turbulence statistics in fully developed channel flow at low Reynolds number. *J. Fluid Mech.* **177**, 133–166.

Madabhushi, R. K. & Vanka, S. P. 1991 Large eddy simulation of turbulence-driven secondary flow in a square duct. *Phys. Fluids* A **3** (11), 2734–2745.

Melling, A. & Whitelaw, J. 1976 Turbulent flow in a rectangular duct. *J. Fluid Mech.* **78**, 289–315.

Nikuradse, J. 1926 Untersuchungen über die Geschwindigkeitsverteilung in turbulenten Strömungen. PhD Thesis, Göttingen. *VDI Forsch.* **281**.

Prandtl, L. 1926 Über die ausgebildete turbulenz. *Verh. 2nd Intl Kong. Fur Tech. Mech., Zurich* [English transl. *NACA Tech. Memo.* 435].

Uhlmann, M., Pinelli, A., Kawahara, G. & Sekimoto, A. 2007 Marginally turbulent flow in a square duct. *J. Fluid Mech.* **588**, 153–162.

Verzicco, R. & Orlandi, P. 1996 A finite-difference scheme for three-dimensional incompressible flows in cylindrical coordinates. *J. Comput. Phys.* **123**, 402–414.